Accelerated Zymonic Acid Formation from Pyruvic Acid at the Interface of Aqueous Nanodroplets

Pyeongeun Kim,[1] Ryan S. Reynolds,[1,2] Alexandra M. Deal,[1] Veronica Vaida,[3] Musahid Ahmed,[1] and Kevin R. Wilson*[,1]

[1]*Chemical Sciences Division, Lawrence Berkeley National Laboratory, Berkeley, California 94720, United States*

[2] *Department of Chemistry, University of California, Berkeley, California 94720, United States*

[3] *Department of Chemistry and CIRES, University of Colorado, Boulder, Colorado, 80309, United States*

*E-mail: krwilson@lbl.gov

Abstract

To explore the role of the liquid interface in mediating reactivity in small compartments, the formation kinetics of zymonic acid (ZA) is measured in submicron aerosols (average radius = 240 nm) using mass spectrometry. Formation of ZA, from a condensation reaction of two pyruvic acid (PA) molecules, proceeds over days in bulk solutions, while in submicron aerosols occurs in minutes. The experimental results are replicated in a kinetic model using an apparent interfacial reaction rate coefficient of $k_{rxn} = 0.9 \pm 0.2 \times 10^{-3}\,M^{-1}\cdot s^{-1}$. The simulation reveals that surface activity of PA coupled with enhanced interfacial reaction rate drive accelerated ZA formation in aerosols. Experimental and simulated results provide compelling evidence that the condensation reaction of PA occurs exclusively at the aerosol interface with a reaction rate coefficient that is enhanced by 4 orders of magnitudes (~10^4) relative to what is estimated for macroscale solutions.

ToC Graphic

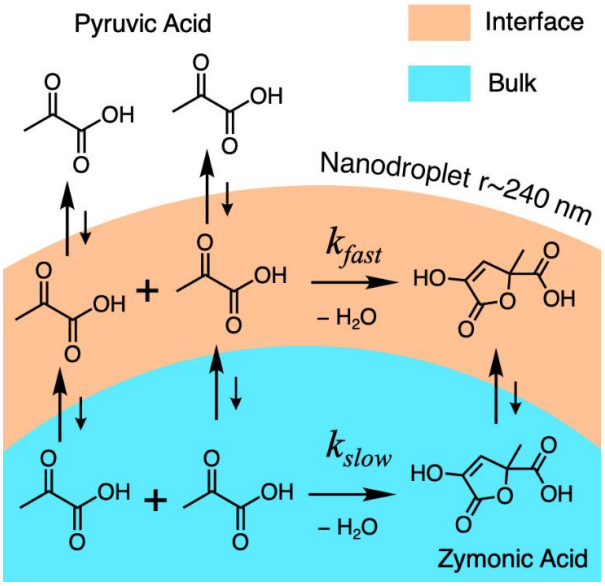

Liquid interfaces play a fundamental role in chemical, biological, and environmental processes.[1–4] Chemical reactions at liquid-liquid and liquid-air interfaces have gained considerable interest over the last decade because of reports of reactions that are accelerated by orders of magnitude compared to those in bulk solutions.[5–8] Recent studies of enhanced reaction rates in microcompartments (*e.g.*, microdroplets and emulsions) suggest that partial or preferential solvation of reactants at the liquid interface and the large surface to volume ratio are key contributors to reaction acceleration.[9–15] In the case of condensation reactions, the kinetic and thermodynamic limitations in bulk solutions due to water elimination have been shown to be reduced at the liquid interfaces.[16,17] Nonetheless, the mechanism for reaction acceleration at liquid interfaces and an accurate kinetic description of the interfacial chemistry remain unclear due to the difficulties of quantifying chemical evolution of (sub)micron-sized systems.

Pyruvic acid (PA), a small alpha-keto acid, is widely studied, abundant in the atmosphere, and contributes to secondary organic aerosol formation by photochemistry.[18–20] The overlap of

solar radiation and the n-π^* transition of PA (300 - 380 nm) has led to extensive studies of PA photochemistry.[21–26] Interestingly, photochemical reactions of PA at the air-water interface are shown to enhance oligomerization over that observed in the bulk solutions.[26] Furthermore, the formation of zymonic acid (ZA, molecular weight = 158 g/mol) from condensation of two PA molecules is observed even in the absence of photochemistry.[26,27] This result is surprising as the bulk reaction requires a highly acidic environment (pH ~ 0) to form ZA with a reaction timescale of several weeks to months.[28,29] Recently, however, Li *et al.* showed that this dark condensation reaction occurs in sessile microdroplets, where ZA formation is relatively rapid (few hours).[30,31] The formation kinetics of ZA, which occur simultaneously with the evaporation of PA and water, are observed to be sigmoidal and size dependent.[30,31]

However, questions remain about the kinetics and mechanism of PA chemistry occurring exclusively at the interface of microdroplets. For example, does the apparent enhanced reaction arise from the interfacial enrichment of reagents and/or a much larger rate coefficient for the surface reaction? Does ZA produced at the surface stay at the surface or partition to the bulk? To answer these questions, the rate coefficient for ZA formation must be quantified within a realistic kinetic description of the bulk-surface partitioning of PA and ZA.[26,27,30] Furthermore, since PA is relatively volatile (vapor pressure at 298K = 175 Pa),[32,33] the mechanism must fully account for the natural competition between evaporation and the reaction of PA.

In this study, interfacial reaction kinetics of PA are investigated by measuring the temporal evolution of [PA] and [ZA] in aqueous aerosols and analyzing the experimental data using a kinetic model that explicitly accounts for surface and bulk reactions.[11,34–39] Submicron aerosols of aqueous PA with NaCl (r_{avg} = 240 nm, Figure S1) are generated using an atomizer, then directed through a variable number of quartz flow tubes in order to change the reaction time from 3 to 70 seconds as

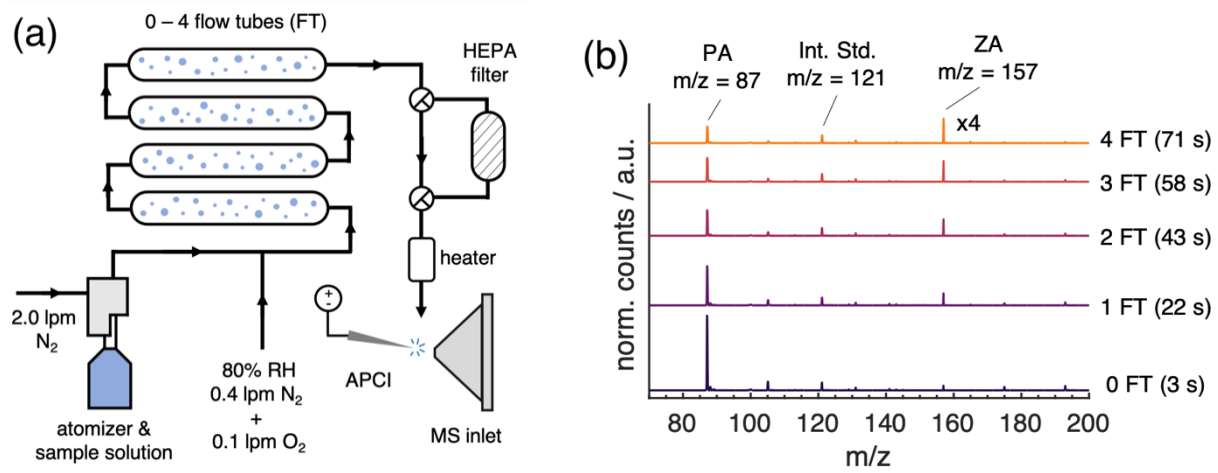

Figure 1: (a) A schematic of the instrumental design for time-resolved mass spectrometric measurements of submicron aqueous aerosols containing PA as a reactant and ZA as a product. APCI denotes atmospheric pressure chemical ionization. RH stands for relative humidity. (b) Time-resolved mass spectra of aerosols generated from aqueous 1M NaCl and 80 mM PA solution (aerosol [NaCl] = 4.6 M and $[PA]_0$ = 370 mM). Varying the number of flow tubes (FTs) enables the measurements of [PA] and [ZA] kinetics in aerosols. Succinic acid d-4 is used as an internal standard (noted as Int. Std. in the spectra).

shown in Figure 1a. NaCl is added to the aerosols to keep the droplet volume constant over the reaction time (*i.e.*, to control water activity). The concentrations of PA and ZA in aerosols are quantified with respect to an internal standard (succinic acid d-4) with low volatility[40] as a function of time by using aerosol atmospheric pressure chemical ionization mass spectrometry (APCI-MS). Time-resolved aerosol mass spectra are shown in Figure 1b. Experimental design and MS analysis is discussed in detail in Supplementary Information (SI Figure S1-3). These aerosol measurements are compared with bulk reactions to ensure that the observed kinetics of PA and ZA occur exclusively in aerosols. A kinetic model is then developed that includes realistic descriptions of bulk-to-interface partitioning, evaporation, and interfacial reaction.[18,32,33,41,42]

The kinetics of [PA] and [ZA] in aerosols ($[PA]_0$ = 370 mM) are shown in Figure 2. The simultaneous decrease of [PA] and formation of [ZA] is observed. After 70 seconds, the [PA] decreased by ~80% (Figure 2a), and ~8 mM of ZA is detected (Figure 2b). This kinetic behavior is consistent for $[PA]_0$ = 230 and 90 mM aerosols (Figure S4). To investigate the difference of

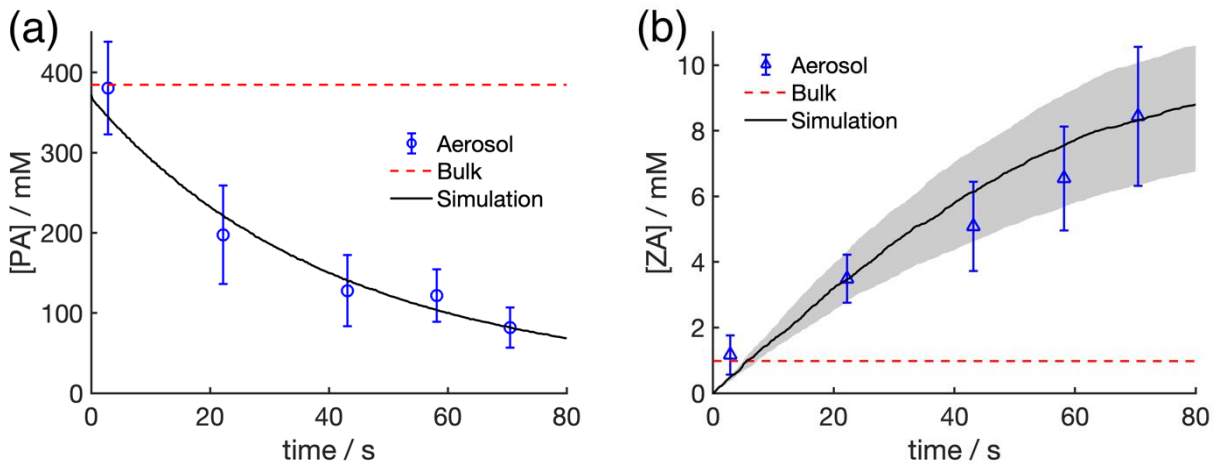

Figure 2: Kinetics of (a) [PA] and (b) [ZA] in aerosols versus residence time in flow tubes ($[PA]_0$ = 370 mM). Every MS measurement is repeated three times, and the error bars represent one standard deviation. Dashed red lines are kinetics of [PA] and [ZA] in a bulk solution. Black solid lines represent simulated results from kinetic modeling discussed later. Grey shaded area in (b) shows ~20% margin of error for the rate constant of ZA formation ($k_{rxn} = 0.9 \pm 0.2 \times 10^{-3}\ M^{-1}\cdot s^{-1}$).

reaction kinetics in aerosols versus bulk solutions, MS measurements are made from bulk solutions with the same composition as aerosols (*i.e.*, $[PA]_0$ = 370 mM and [NaCl] = 4.6 M) (Figure S5). After 2.5 hours the MS of the bulk solution does not show significant changes in [PA] and [ZA], and the linear fits to the bulk data are shown for comparison as dashed lines in Figure 2a and b. The result from this control experiment agrees with previous literature where the timescale of ZA formation in bulk solutions ranges from weeks to months.[28,29] These observations clearly demonstrate that the formation of ZA is favored in small droplets, likely because the air-water interface is a substantial fraction of the reaction environment.[27,30]

Additionally, since the formation of ZA from two PA molecules requires the elimination of water, the role of rapid water evaporation during the initial equilibration process (*i.e.* as the droplets exit the atomizer) to 80% RH is evaluated. As a control experiment, aerosols are generated from the solutions with the PA and NaCl concentrations identical to the equilibrated conditions at RH = 80% ([PA] = 370 mM and [NaCl] = 4.6 M), thus aerosols experience no rapid evaporation. The aerosols are then routed through the same set of flow tubes with ~70 seconds reaction time as

done for the data shown in Figure 2. The results still show the formation of ZA with increasing reaction time indicating that rapid initial water evaporation is not required to form ZA (Figure S6). It is also confirmed that the hydrolysis of ZA back into 2 pyruvic acid molecules is negligible under our conditions by running aerosols with ZA only ($[ZA]_0$ = 41 mM) in the flow tubes (Figure S7). We find no noticeable changes in [ZA] or the formation of PA with reaction time for aerosols or in bulk solutions over two hours. This result suggests that the reverse reaction rate of the ZA formation is negligible compared to the forward reaction.

In addition to PA (m/z = 87) and ZA (m/z = 157), the kinetics of the smaller peaks (m/z = 105, 113, 175, and 193) in MS spectra (Figure 1b) are shown in Figure S8. The ZA fragment peak at m/z = 113 ($ZA\text{-}CO_2\text{-}H^-$; identified by CID data, see Figure S2) increases as a function of time similar to the main ZA peak (m/z = 157). The m/z = 105 peak, corresponding to the hydrated diol of pyruvic acid, 2,2-dihydroxypropanoic acid (2,2-DHPA),[26,43] exhibits decay kinetics similar to PA. Interestingly, the m/z = 175 peak, assigned to parapyruvic acid,[26,42,44] also shows a steady decrease with reaction time, which warrants further discussion.

Parapyruvic acid (PPA) has been proposed as a reaction intermediate during the formation of ZA as shown in (R1) where both steps are acid-catalyzed.[27]

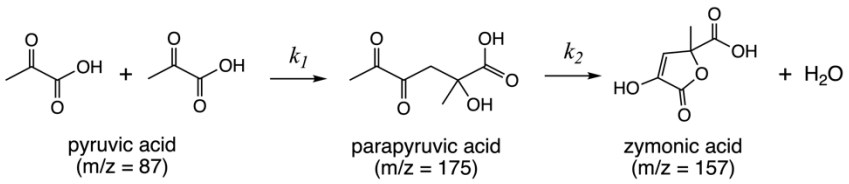

(R1)

However, in the timescale of our experiments, no significant buildup of PPA as an intermediate in aerosols is observed (Figure S8). This suggests that any PPA formed is rapidly lost to reaction, meaning the unimolecular ring formation step (k_2) would be relatively fast, and the first bimolecular reaction (k_1) is likely the rate determining step. Thus, we can simplify the proposed

mechanism (R1) to (R2), where ZA is directly formed from the bimolecular condensation of PA with a second-order rate constant, k_{rxn}.

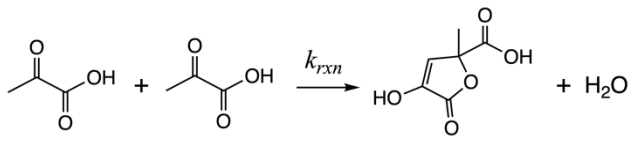

(R2)

As observed in Figure 2, disappearance of PA and formation of ZA occurs simultaneously in the aerosol environment. This likely occurs at the air-water interface, which is consistent with the observations from other studies.[24,30] Interestingly, the measured kinetic data suggest that the major contribution to the decrease of [PA] over time is evaporation. In the case of $[PA]_0$ = 370 mM aerosols, for example, the [PA] is reduced to 80 mM after 70 seconds (Figure 2a), whereas the [ZA] that is formed is only ~8 mM (Figure 2b). Therefore, out of 290 mM [PA], only 16 mM of [PA] is consumed in the formation of ZA, whereas the remaining 274 mM of [PA] is lost to evaporation. To unravel the competition between reaction and evaporation at the aerosol interface and further quantify the rate constants for each process, a kinetic model is developed.

A two-compartment model representing the interface and bulk of an aerosol droplet and a mechanistic description of the partitioning, evaporation, and reaction kinetics of PA and ZA is shown in Figure 3.[11,34–39] Since the aerosols remain in the liquid phase throughout the experimental condition at 80% RH,[45] it is reasonable to assume they have a spherical geometry with surface to volume ratio (S:V) of $3/r$, where r is the volume-averaged radius of the polydisperse aerosols (240 nm, Figure S1). A box model with interface and bulk compartments (Figure 3a) is used to set the stage for stochastic simulation of the reaction and partitioning of the species in the aerosols. The interface compartment is defined as 1 nm thick with a 1 nm^2 base area. The 1 nm interfacial thickness is consistent with the molecular dynamics (MD) simulation studies of water interfaces.[38,46,47] The bulk compartment has 1 nm^2 base area with $3/r$ height to reflect the S:V ratio

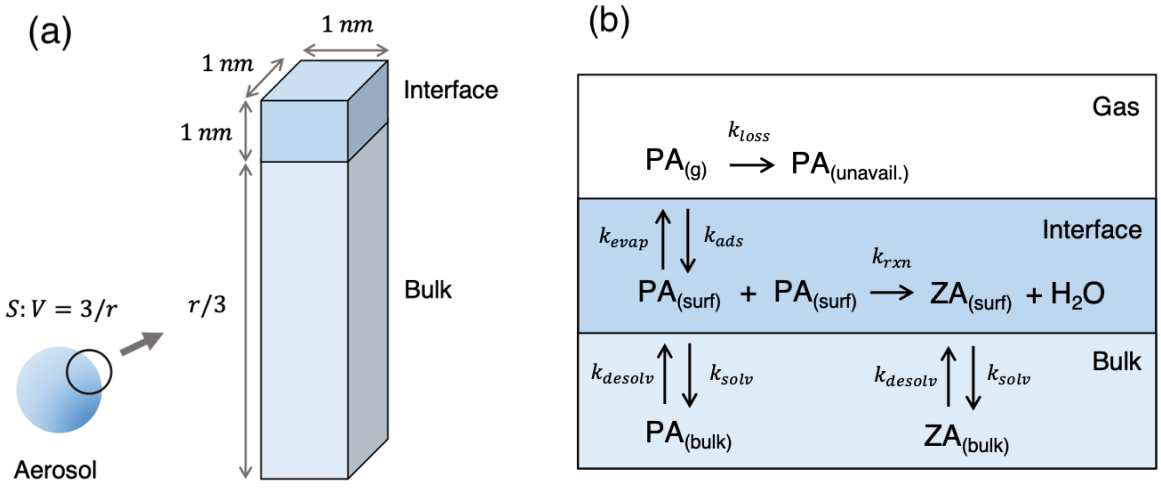

Figure 3: A graphical illustration of the model used for simulating reaction kinetics in submicron aerosols. (a) A spherical geometry of aerosols is reduced to a box model in stochastic simulation. Volumes of the interface and bulk compartments are defined as 1 x 1 x 1 nm^3 and 1 x 1 x $r/3\,nm^3$, respectively, retaining the surface to volume ratio of a sphere ($3/r$). (b) Mechanism of the bulk-interface and interface-gas partitioning of PA as well as the condensation reaction at the interface of aerosols.

of a sphere in the box model. We use Kinetiscope®, a stochastic reaction-diffusion simulator, to model the kinetics of PA and ZA.[48,49] Detailed settings and the values of the input parameters for the simulations are listed in Table S1.

Figure 3b shows the elementary kinetic steps that describe 1) interface-bulk partitioning of PA and ZA, 2) evaporation and adsorption of PA between interface and gas phase, and 3) formation of ZA at the interface by condensation of two PA molecules. Although PA and ZA can exist in different forms in aqueous solution,[28,50] for simplicity only the keto form of PA and closed enol form of ZA are considered in interfacial reactions as done in other studies.[30,42] The interface-bulk partitioning, or surface activity, of PA is described by solvation (k_{solv}, interface to bulk) and desolvation (k_{desolv}, bulk to interface) rate constants. To quantify the concentration of PA at the interface ($[PA]_{(surf)}$) available for evaporation and reaction the value of the equilibrium partitioning constant ($K_{eq}^{PA} = k_{desolv}/k_{solv}$, in units of M^{-1}) is needed. The value of K_{eq}^{PA} can be obtained by fitting the Langmuir/Szyszkowski adsorption model to the experimentally measured surface tension of

an aqueous PA solution.[42]

The Langmuir/Szyszkowski equation of state (EOS) is,

$$\gamma - \gamma_{water} = \Gamma_{\infty}^{PA} \cdot R \cdot T \cdot \ln(1-\theta) \quad (1)$$

where γ is the surface tension of PA solution ($N \cdot m^{-1}$), γ_{water} is the surface tension of water (72×10^{-3} $N \cdot m^{-1}$),[51] Γ_{∞}^{PA} is the maximum surface concentration of PA (4.3×10^{-10} $moles \cdot cm^{-2}$),[52] R is the gas constant, and T is the temperature (298 K). From the Langmuir equation, the fractional occupancy of PA at the interface (θ) and K_{eq}^{solv} is,

$$\theta = \frac{K_{eq}^{solv}[PA]_{bulk}}{1+K_{eq}^{solv}[PA]_{bulk}} . \quad (2)$$

The value K_{eq}^{PA} = 28.5 M^{-1} is obtained by fitting equation (1) to the surface tension data of aqueous PA solutions (Figure S9).[42] For partitioning of ZA, Gordon *et al.*[42] reported that PA and ZA have a similar surface propensity in MD simulations, thus we assume an identical value of K_{eq}^{ZA}= 28.5 M^{-1}. From K_{eq}^{PA}, values of k_{solv} and k_{desolv} for PA and ZA are defined as 100 s^{-1} and 2850 $M^{-1} \cdot s^{-1}$, respectively, and the exact value has minimal impact on simulated results (Figure S10). A value of k_{solv} = 100 s^{-1} is consistent with solvation kinetics of similar-sized organic acids measured by Bleys and Joos, and k_{desolv} is calculated from $k_{desolv} = K_{eq}^{solv} \cdot k_{solv}$.[52] Finally, Γ_{∞}^{PA} (4.3×10^{-10} $moles \cdot cm^{-2}$) is converted into a maximum volumetric concentration of PA at the interface ($[PA]_{surf}^{max}$, unit: M) by,

$$[PA]_{surf}^{max} = \frac{\Gamma_{\infty}^{PA}}{\delta} \cdot \theta \approx 4.3\ M \quad (3)$$

where δ is the interfacial thickness defined as 1 nm as discussed before (Figure 3a). The value of 4.3 M can also be interpreted as a concentration of available adsorption sites at the interface, where PA and ZA molecules occupy one and two sites, respectively. The exact values of k_{solv}, k_{desolv}, and

$[PA]_{surf}^{max}$ derived here are used in the simulation to reproduce the bulk-interface partitioning behavior of PA and ZA (Figure 3b).

The evaporation rate of PA in aqueous aerosols is described by the Hertz-Knudsen equation,[49,53,54]

$$J = \frac{\alpha p_{vap}}{\sqrt{2\pi m k_B T}} \quad (4)$$

where J is molecular flux (units: $molec \cdot m^{-2} \cdot s^{-1}$), p_{vap} the saturation vapor pressure of PA ($175\ Pa$), α is the evaporation coefficient (assumed as 1), m is the mass of a PA molecule ($1.46 \times 10^{-25}\ kg$), and k_B is the Boltzmann constant. The [PA] in the aerosol is relatively dilute (*i.e.*, mM) so the Henry's law constant can be used to substitute p_{vap},

$$\frac{J}{[PA]} = \frac{1/H_{PA}}{\sqrt{2\pi m k_B T}}. \quad (5)$$

From prior literature, H_{PA} for PA is $3.06\ mol \cdot kg^{-1} \cdot Pa^{-1}$.[32,33,41] Note the units of the left hand side of the equation are $m \cdot s^{-1}$. To obtain the evaporation rate constant in units of s^{-1}, the geometry of the simulation (*i.e.*, S:V ratio) is needed to account for surface availability for evaporation. Finally, k_{evap} is expressed as,

$$k_{evap} = \frac{A_{sim}}{V_{sim}} \frac{1/H_{PA}}{\sqrt{2\pi m k_B T}} \quad (6)$$

where A_{sim} and V_{sim} are surface area and volume of the simulation geometry, respectively, as shown in Figure 3a. Equation (6) yields $k_{evap} = 110\ s^{-1}$ for r = 240 nm aerosols. The rate constant for gas phase to interface adsorption (k_{ads}) can be computed in a similar manner, using the Henry's law constant. In a fully enclosed system at equilibrium, $k_{ads} = k_{evap}$. Although the flow tube reactors are fully enclosed, [PA] is observed to decrease over time (Figure 2a). This decrease in [PA] cannot be fully explained by reactive loss, as discussed above, suggesting that PA is also lost to the reactor walls. Wall loss of gas phase molecules or aerosols are commonly observed and quantified in

experimental studies utilizing flow tubes or reaction chambers.[55,56] In the kinetic model, a rate constant for wall loss (k_{loss}) is included as an adjustable parameter. A value of k_{loss} = 0.1 s^{-1} best replicates the measured kinetics of [PA] at three different initial PA concentrations as shown in Figure 2a and Figure S4.

Lastly, the rate constant of ZA formation is described in the model as k_{rxn}. As discussed previously, this reaction is assumed to follow bimolecular reaction kinetics so the units of k_{rxn} are $M^{-1} \cdot s^{-1}$. Additionally, we assume the condensation reaction occurs exclusively at the interface, as shown in Figure 3b, as a negligible quantity of ZA is formed in bulk PA solutions (Figure 2a and Figure S4). Therefore, k_{rxn} remains as the only unknown parameter for simulating ZA formation kinetics since the bulk-interface partitioning and evaporation of PA and ZA are constrained by K_{eq}^{PA}, K_{eq}^{ZA} and $[PA]_{surf}^{max}$. A value of k_{rxn} = 0.9 ± 0.2 × 10^{-3} $M^{-1} \cdot s^{-1}$ best replicates the entire experimental data set as shown in Figure 2b and Figure S4.

In addition to reproducing MS data, the simulated results can be used to evaluate the contributions from bulk and interface regions to the overall observed kinetics. For example, Figure 4 shows the interplay between the interface and bulk by separating the kinetics of [PA] and [ZA] in each compartment for the $[PA]_0$ = 370 mM data set (see Figure S10 for $[PA]_0$ = 90 and 230 mM aerosols). At the start of the simulation (t ~ 0 s), rapid partitioning of PA from the bulk to the interface is observed (Figure 4a). This partitioning leads to the depletion of $[PA]_{bulk}$, which is more significant as $[PA]_0$ decreases (Figure S11). It can be also seen in Figure 4a that the consumption rate of [PA] is more significant in the bulk compartment compared to the interface, which can be explained by evaporation. Due to the surface activity of PA (K_{eq}^{PA}= 28.5 M^{-1}), each time a PA molecule evaporates from the interface to the gas phase, the adsorption site is quickly replaced by another PA from the bulk.

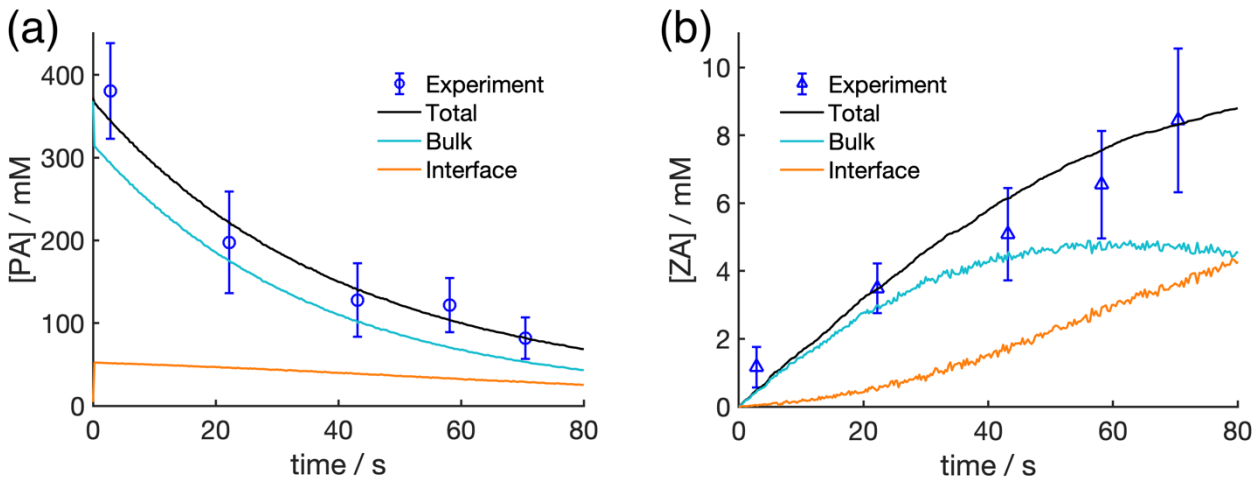

Figure 4: The detailed simulated results depicting the interface and bulk contributions to the (a) [PA] and (b) [ZA] kinetics in $[PA]_0$ = 370 mM aerosols. Blue circles represent the MS-measured concentrations. Error bars are standard deviations of three measurements. Solid black lines are simulated total concentrations of PA and ZA in aerosols as shown in Figure 2a. Teal and orange lines are contributions from the bulk and the interface compartments, respectively.

Unlike the overall decrease of PA in each compartment, the formation kinetics of ZA exhibit a unique behavior. Figure 4b shows that ZA molecules predominantly partition to the bulk compartment during the early stages of the reaction (up to ~40 seconds) although the formation of ZA is restricted to the interface. Even though the surface propensities of ZA and PA are assumed to be identical, the abundance of PA and the limited number of available sites at the interface lead to the majority of ZA molecules formed at the interface to partition into bulk. However, after ~60 seconds, the ZA contribution from the bulk decreases while the coverage of ZA at the interface steadily increases. This trend is due to the decrease of PA molecules at the interface, which are consumed by ZA formation, evaporation, and wall loss leaving more sites at the interface for ZA, thus increasing its bulk to interface partitioning.

Although the apparent rate constant of dark ZA formation in aerosols is obtained in this study, the rate constant for ZA formation in bulk solutions has not been reported to our knowledge. Only the timescale of acid-catalyzed ZA formation is reported by Düwel *et al.*, which is 20-30 days in highly acidic solutions (1 M HCl, pH ~ 0).[29] From these observations, one can roughly

estimate the value of the rate constant in bulk solutions to be $k_{rxn,bulk} \sim 4.0 \times 10^{-8}\ M^{-1} \cdot s^{-1}$ (see Figure S12). This estimate assumes a 40% yield of ZA after 30 days as reported.[29] Using this value in the simulations of $[PA]_0$ = 370 mM aerosols would result in 1.1 μM (micromolar) of ZA formation after 100 seconds of reaction time as shown in Figure S11, which cannot explain the observed ~10 mM of [ZA] in Figure 2b. We suggest this substantial degree of reaction acceleration of ZA formation in aerosols (factor of ~10^4 to 10^5) is due both to an enhanced reaction rate at the interface and the enrichment of PA at the interface.[42] It is worth noting the value of k_{rxn} derived in this study is ~2 orders of magnitude smaller than the value obtained from the kinetic modeling of sessile microdroplets, although the direct comparison is difficult because of different experimental conditions such as solid substrate, size, droplet pH, and reaction steps.[31]

There are a number of condensation reactions, such as peptide bond formation and imine formation, which are also shown to be enhanced at the interface, possibly due to partial solvation and transition state stabilization.[5,12,16,17] For example, the enhanced rate of imine synthesis at the interface of microdroplets investigated by Fallah-Araghi *et al.* and our group is on the order of 10^{-4} to $10^{-3}\ M^{-1} \cdot s^{-1}$,[5,11] similar to the apparent value obtained for ZA formation in this study (k_{rxn} = 0.9 ± 0.2 × $10^{-3}\ M^{-1} \cdot s^{-1}$). In addition, the ZA production via photochemical reactions of PA is also significantly enhanced at the interface compared to bulk, according to the study by Kappes *et al.*[26] These findings, along with our analysis, strongly suggest that the formation of ZA in aerosols is another example of a water-eliminating reaction preferentially occurring at the liquid interface.

Moreover, the enhanced concentration of surface-active reactants at the interface is considered one of the key factors of accelerated reaction kinetics in small systems.[11,15,57] To examine the role of bulk to interface partitioning of PA (*i.e.*, K_{eq}^{PA}) on the formation of ZA and loss of PA in aerosols, simulated kinetics with varying K_{eq}^{PA} and k_{rxn} are shown in Figure 5. The

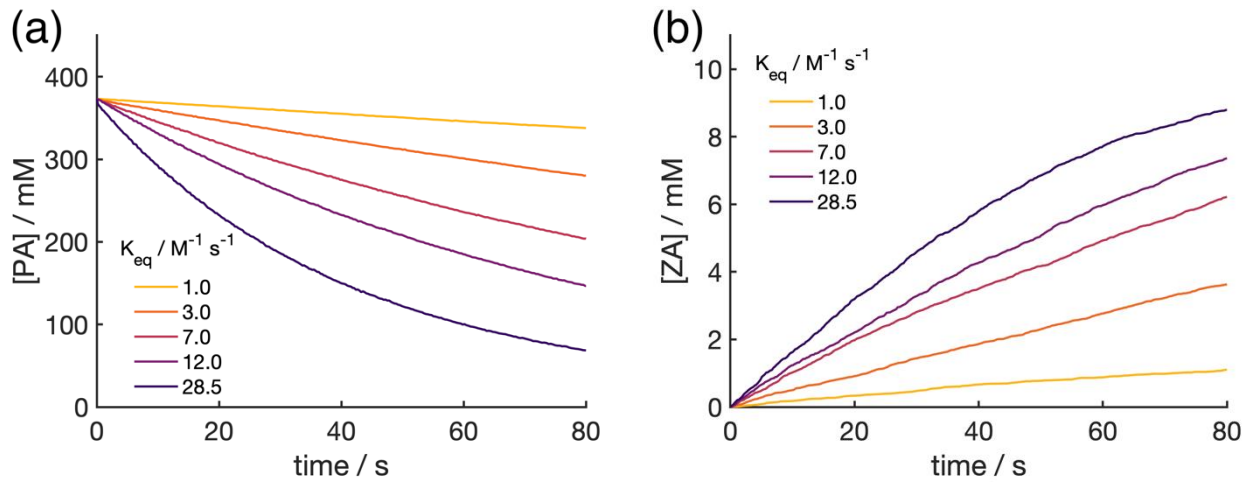

Figure 5: Simulated kinetics of (a) [PA] and (b) [ZA] assuming different values for the bulk to interface equilibrium constant of PA (K_{eq}^{PA}) from 1 to 28.5 M^{-1} while the rate of ZA formation remains constant ($k_{rxn} = 0.9 \times 10^{-3}\ M^{-1} \cdot s^{-1}$). The decrease of [PA] as well as the increase of [ZA] are significantly slower with lower K_{eq}^{PA} values, indicating that the surface activity of PA is crucial for ZA formation in aerosols.

magnitude of K_{eq}^{PA} has a substantial impact on the simulated kinetics of [PA] and [ZA] as both the evaporation of PA (Figure 5a) and formation of ZA (Figure 5b) at the interface are suppressed when K_{eq}^{PA} is decreased. This tendency clearly shows that the surface activity of PA in aqueous systems is one of the underlying causes for accelerated formation of ZA. The effect of surface activity of PA on reaction acceleration is especially pronounced in this study because PA concentrations in the bulk compartment stay relatively low compared to the interface ($[PA]_{bulk}$ < 400 mM vs $[PA]_{interface}$ = 4.3 M), and the reactions occur exclusively at the interface.

In conclusion, the accelerated formation of ZA via PA condensation reaction in aerosols is measured by time-resolved MS analysis. To explain the observed decrease of [PA] and increase of [ZA] in aerosols, a kinetic model including droplet geometry, bulk to interface partitioning, interfacial reaction, and evaporation is developed. By fitting the kinetic simulation to the experimental data, the rate constant for the formation of ZA at the interface of aqueous aerosols ($k_{rxn} = 0.9 \pm 0.2 \times 10^{-3}\ M^{-1} \cdot s^{-1}$) is obtained, and is estimated to be ~4 orders of magnitudes larger than the reaction rate in bulk solutions. Simulated results reveal the bulk to interface partitioning

of PA and interface-enhanced condensation reaction lead to the observed accelerated ZA formation in nanodroplets. Regarding the inherent reaction acceleration of PA at the liquid interface, there is an important lingering question: what drives the reaction rate constant at the interface to be significantly higher than the one in bulk? Although the exact reason for the enhancement is elusive, there are possible explanations based on non-trivial physical properties at the interface including electrostatic potential fluctuation, molecular orientation, surface acidity, and partial solvation.[12,15,58,59] Future studies about the detailed mechanism of dark PA condensation and the energetics of the enhanced chemical reaction at the liquid-air interface will greatly benefit the current understanding of the unique reactions in microcompartments under debate. Moreover, surface-sensitive techniques such as X-ray photoelectron spectroscopy[60,61] and vibrational sum-frequency generation spectroscopy[62] could be used to directly compare reaction kinetics in liquid interface versus bulk.

Acknowledgements

The authors gratefully acknowledge support from the Director, Office of Energy Research, Office of Basic Energy Sciences, Chemical Sciences Division of the U.S. Department of Energy under contract No. DE-AC02-05CH11231. The Condensed Phase and Interfacial Molecular Sciences Program supported the model development and Gas Phase Chemical Physics program supported the Atmospheric Pressure Chemical Ionization measurements.

Associated Content

Supporting Information

The supporting information is available free of charge at: doi.xx

Data of aerosol size, CID-MS spectra of ZA, calibration curves for MS, bulk control experiments,

fitting Langmuir equation to surface tension of PA, estimated ZA formation rate in bulk, molality (m) to molarity (M) conversion for PA, description of geometry for sessile microdroplet, simulated radius of sessile microdroplet over time, detailed explanation of kinetic model for sessile microdroplet, and tabulated simulation parameters and rate constants (PDF).

Author Information

Corresponding Author

Kevin R. Wilson - *Chemical Sciences Division, Lawrence Berkeley National Laboratory, 1 Cyclotron Road, Berkeley, California, 94720, United States*; orcid.org/0000-0003-0264-0872;

Authors

Pyeongeun Kim - *Chemical Sciences Division, Lawrence Berkeley National Laboratory, 1 Cyclotron Road, Berkeley, California, 94720, United States;* orcid.org/0000-0002-4718-4770;

Ryan S. Reynolds - *Chemical Sciences Division, Lawrence Berkeley National Laboratory, 1 Cyclotron Road, Berkeley, California, 94720, United States; and Department of Chemistry, University of California, Berkeley, California, 94720, United States;*

Alexandra M. Deal - *Chemical Sciences Division, Lawrence Berkeley National Laboratory, 1 Cyclotron Road, Berkeley, California, 94720, United States*;

Veronica Vaida – *Department of Chemistry and CIRES, University of Colorado, Boulder, Colorado, 80309, United States*;

Musahid Ahmed - *Chemical Sciences Division, Lawrence Berkeley National Laboratory, 1 Cyclotron Road, Berkeley, California, 94720, United States*; orcid.org/0000-0003-1216-673X;

References

(1) Eisenthal, K. B. Liquid Interfaces. *Acc. Chem. Res.* **1993**, *26* (12), 636–643.

(2) Jungwirth, P.; Tobias, D. J. Molecular Structure of Salt Solutions: A New View of the Interface with Implications for Heterogeneous Atmospheric Chemistry. *J. Phys. Chem. B* **2001**, *105* (43), 10468–10472.

(3) Ni, L.; Yu, C.; Wei, Q.; Liu, D.; Qiu, J. Pickering Emulsion Catalysis: Interfacial Chemistry, Catalyst Design, Challenges, and Perspectives. *Angewandte Chemie* **2022**, *134* (30), e202115885.

(4) George, I. J.; Abbatt, J. P. D. Heterogeneous Oxidation of Atmospheric Aerosol Particles by Gas-Phase Radicals. *Nature Chem* **2010**, *2* (9), 713–722.

(5) Fallah-Araghi, A.; Meguellati, K.; Baret, J.-C.; Harrak, A. E.; Mangeat, T.; Karplus, M.; Ladame, S.; Marques, C. M.; Griffiths, A. D. Enhanced Chemical Synthesis at Soft Interfaces: A Universal Reaction-Adsorption Mechanism in Microcompartments. *Phys. Rev. Lett.* **2014**, *112* (2), 028301.

(6) Jordan, C. J. C.; Lowe, E. A.; Verlet, J. R. R. Photooxidation of the Phenolate Anion Is Accelerated at the Water/Air Interface. *J. Am. Chem. Soc.* **2022**, *144* (31), 14012–14015.

(7) Tian, Y.-M.; Silva, W.; Gschwind, R. M.; König, B. Accelerated Photochemical Reactions at Oil-Water Interface Exploiting Melting Point Depression. *Science* **2024**, *383* (6684), 750–756.

(8) Gong, C.; Yuan, X.; Xing, D.; Zhang, D.; Martins-Costa, M. T. C.; Anglada, J. M.; Ruiz-López, M. F.; Francisco, J. S.; Zhang, X. Fast Sulfate Formation Initiated by the Spin-Forbidden Excitation of SO_2 at the Air–Water Interface. *J. Am. Chem. Soc.* **2022**, *144* (48), 22302–22308.

(9) Rovelli, G.; Jacobs, M. I.; Willis, M. D.; Rapf, R. J.; Prophet, A. M.; Wilson, K. R. A Critical Analysis of Electrospray Techniques for the Determination of Accelerated Rates and Mechanisms of Chemical Reactions in Droplets. *Chem. Sci.* **2020**, *11* (48), 13026–13043.

(10) Wei, Z.; Li, Y.; Cooks, R. G.; Yan, X. Accelerated Reaction Kinetics in Microdroplets: Overview and Recent Developments. *Annu. Rev. Phys. Chem.* **2020**, *71* (1), 31–51.

(11) Wilson, K. R.; Prophet, A. M.; Rovelli, G.; Willis, M. D.; Rapf, R. J.; Jacobs, M. I. A Kinetic Description of How Interfaces Accelerate Reactions in Micro-Compartments. *Chem. Sci.* **2020**, *11* (32), 8533–8545.

(12) Martins-Costa, M. T. C.; Ruiz-López, M. F. Electrostatics and Chemical Reactivity at the Air–Water Interface. *J. Am. Chem. Soc.* **2023**, *145* (2), 1400–1406.

(13) Xia, D.; Chen, J.; Xie, H.-B.; Zhong, J.; Francisco, J. S. Counterintuitive Oxidation of Alcohols at Air–Water Interfaces. *J. Am. Chem. Soc.* **2023**, *145* (8), 4791–4799.

(14) Wilson, K.; Prophet, A. Chemical Kinetics in Microdroplets. *Annu. Rev. Phys. Chem.* **2024**, *75*.

(15) Ben-Amotz, D. Interfacial Chemical Reactivity Enhancement. *The Journal of Chemical Physics* **2024**, *160* (8), 084704.

(16) Griffith, E. C.; Vaida, V. In Situ Observation of Peptide Bond Formation at the Water–Air Interface. *Proc. Natl. Acad. Sci. U.S.A.* **2012**, *109* (39), 15697–15701.

(17) Deal, A. M.; Rapf, R. J.; Vaida, V. Water–Air Interfaces as Environments to Address the Water Paradox in Prebiotic Chemistry: A Physical Chemistry Perspective. *J. Phys. Chem. A* **2021**, *125* (23), 4929–4942.

(18) Andreae, M. O.; Talbot, R. W.; Li, S.-M. Atmospheric Measurements of Pyruvic and Formic Acid. *J. Geophys. Res.* **1987**, *92* (D6), 6635.

(19) Talbot, R. W.; Andreae, M. O.; Berresheim, H.; Jacob, D. J.; Beecher, K. M. Sources and Sinks of Formic, Acetic, and Pyruvic Acids over Central Amazonia: 2. Wet Season. *J. Geophys. Res.* **1990**, *95* (D10), 16799–16811.

(20) Eger, P. G.; Schuladen, J.; Sobanski, N.; Fischer, H.; Karu, E.; Williams, J.; Riva, M.; Zha, Q.; Ehn, M.; Quéléver, L. L. J.; Schallhart, S.; Lelieveld, J.; Crowley, J. N. Pyruvic Acid in the Boreal Forest: Gas-Phase Mixing Ratios and Impact on Radical Chemistry. *Atmospheric Chemistry and Physics* **2020**, *20* (6), 3697–3711.

(21) Horowitz, A.; Meller, R.; Moortgat, G. K. The UV–VIS Absorption Cross Sections of the α-Dicarbonyl Compounds: Pyruvic Acid, Biacetyl and Glyoxal. *Journal of Photochemistry and Photobiology A: Chemistry* **2001**.

(22) Griffith, E. C.; Carpenter, B. K.; Shoemaker, R. K.; Vaida, V. Photochemistry of Aqueous Pyruvic Acid. *Proc. Natl. Acad. Sci. U.S.A.* **2013**, *110* (29), 11714–11719.

(23) Reed Harris, A. E.; Ervens, B.; Shoemaker, R. K.; Kroll, J. A.; Rapf, R. J.; Griffith, E. C.; Monod, A.; Vaida, V. Photochemical Kinetics of Pyruvic Acid in Aqueous Solution. *J. Phys. Chem. A* **2014**, *118* (37), 8505–8516.

(24) Reed Harris, A. E.; Pajunoja, A.; Cazaunau, M.; Gratien, A.; Pangui, E.; Monod, A.; Griffith, E. C.; Virtanen, A.; Doussin, J.-F.; Vaida, V. Multiphase Photochemistry of Pyruvic Acid under Atmospheric Conditions. *J. Phys. Chem. A* **2017**, *121* (18), 3327–3339.

(25) Luo, M.; Shemesh, D.; Sullivan, M. N.; Alves, M. R.; Song, M.; Gerber, R. B.; Grassian, V. H. Impact of pH and NaCl and $CaCl_2$ Salts on the Speciation and Photochemistry of Pyruvic Acid in the Aqueous Phase. *J. Phys. Chem. A* **2020**, *124* (25), 5071–5080.

(26) Kappes, K. J.; Deal, A. M.; Jespersen, M. F.; Blair, S. L.; Doussin, J.-F.; Cazaunau, M.;

Pangui, E.; Hopper, B. N.; Johnson, M. S.; Vaida, V. Chemistry and Photochemistry of Pyruvic Acid at the Air–Water Interface. *J. Phys. Chem. A* **2021**, *125* (4), 1036–1049.

(27) Petters, S. S.; Hilditch, T. G.; Tomaz, S.; Miles, R. E. H.; Reid, J. P.; Turpin, B. J. Volatility Change during Droplet Evaporation of Pyruvic Acid. *ACS Earth Space Chem.* **2020**, *4* (5), 741–749.

(28) Perkins, R. J.; Shoemaker, R. K.; Carpenter, B. K.; Vaida, V. Chemical Equilibria and Kinetics in Aqueous Solutions of Zymonic Acid. *J. Phys. Chem. A* **2016**, *120* (51), 10096–10107.

(29) Düwel, S.; Hundshammer, C.; Gersch, M.; Feuerecker, B.; Steiger, K.; Buck, A.; Walch, A.; Haase, A.; Glaser, S. J.; Schwaiger, M.; Schilling, F. Imaging of pH in Vivo Using Hyperpolarized 13C-Labelled Zymonic Acid. *Nat Commun* **2017**, *8* (1), 15126.

(30) Li, M.; Boothby, C.; Continetti, R. E.; Grassian, V. H. Size-Dependent Sigmoidal Reaction Kinetics for Pyruvic Acid Condensation at the Air–Water Interface in Aqueous Microdroplets. *J. Am. Chem. Soc.* **2023**, *145* (41), 22317–22321.

(31) Li, M.; Yang, S.; Rathi, M.; Kumar, S.; Dutcher, C. S.; Grassian, V. H. Enhanced Condensation Kinetics in Aqueous Microdroplets Driven by Coupled Surface Reactions and Gas-Phase Partitioning. *Chem. Sci.* **2024**, *15* (33), 13429–13441.

(32) Khan, I.; Brimblecombe, P. Henry's Law Constants of Low Molecular Weight (<130) Organic Acids. *Journal of Aerosol Science* **1992**, *23*, 897–900.

(33) Khan, I.; Brmblecombe, P.; Clegg, S. L. The Henry's Law Constants of Pyruvic and Methacrylic Acids. *Environmental Technology* **1992**, *13* (6), 587–593.

(34) Houle, F. A.; Miles, R. E. H.; Pollak, C. J.; Reid, J. P. A Purely Kinetic Description of the Evaporation of Water Droplets. *The Journal of Chemical Physics* **2021**, *154* (5), 054501.

(35) Wilson, K. R.; Prophet, A. M.; Willis, M. D. A Kinetic Model for Predicting Trace Gas Uptake and Reaction. *J. Phys. Chem. A* **2022**, *126* (40), 7291–7308.

(36) Willis, M. D.; Wilson, K. R. Coupled Interfacial and Bulk Kinetics Govern the Timescales of Multiphase Ozonolysis Reactions. *J. Phys. Chem. A* **2022**, *126* (30), 4991–5010.

(37) Brown, E. K.; Rovelli, G.; Wilson, K. R. pH Jump Kinetics in Colliding Microdroplets: Accelerated Synthesis of Azamonardine from Dopamine and Resorcinol. *Chem. Sci.* **2023**, *14* (23), 6430–6442.

(38) Prophet, A. M.; Polley, K.; Van Berkel, G. J.; Limmer, D. T.; Wilson, K. R. Iodide Oxidation by Ozone at the Surface of Aqueous Microdroplets. *Chem. Sci.* **2024**, *15* (2), 736–756.

(39) Houle, F. A.; Hinsberg, W. D.; Wilson, K. R. Oxidation of a Model Alkane Aerosol by OH Radical: The Emergent Nature of Reactive Uptake. *Phys. Chem. Chem. Phys.* **2015**, *17* (6),

4412–4423.

(40) Wallace, B. J.; Mongeau, M. L.; Zuend, A.; Preston, T. C. Impact of pH on Gas-Particle Partitioning of Semi-Volatile Organics in Multicomponent Aerosol. *Environ. Sci. Technol.* **2023**, *57* (44), 16974–16988.

(41) Sander, R. Compilation of Henry's Law Constants (Version 4.0) for Water as Solvent. *Atmospheric Chemistry and Physics* **2015**, *15* (8), 4399–4981.

(42) Gordon, B. P.; Moore, F. G.; Scatena, L. F.; Richmond, G. L. On the Rise: Experimental and Computational Vibrational Sum Frequency Spectroscopy Studies of Pyruvic Acid and Its Surface-Active Oligomer Species at the Air–Water Interface. *J. Phys. Chem. A* **2019**, *123* (49), 10609–10619.

(43) Barquilla, M. D. P.; Mayes, M. L. Role of Hydrogen Bonding in Bulk Aqueous Phase Decomposition, Complexation, and Covalent Hydration of Pyruvic Acid. *Phys. Chem. Chem. Phys.* **2022**, *24* (41), 25151–25170.

(44) Rapf, R. J.; Perkins, R. J.; Carpenter, B. K.; Vaida, V. Mechanistic Description of Photochemical Oligomer Formation from Aqueous Pyruvic Acid. *J. Phys. Chem. A* **2017**, *121* (22), 4272–4282.

(45) Braun, C.; Krieger, U. K. Two-Dimensional Angular Light-Scattering in Aqueous NaCl Single Aerosol Particles during Deliquescence and Efflorescence. *Opt. Express* **2001**, *8* (6), 314.

(46) Herdes, C.; Ervik, Å.; Mejía, A.; Müller, E. A. Prediction of the Water/Oil Interfacial Tension from Molecular Simulations Using the Coarse-Grained SAFT-γ Mie Force Field. *Fluid Phase Equilibria* **2018**, *476*, 9–15.

(47) Martins-Costa, M. T. C.; Ruiz-López, M. F. Probing Solvation Electrostatics at the Air–Water Interface. *Theor Chem Acc* **2023**, *142* (3), 29.

(48) Hinsberg, W.; Houle, F. Kinetiscope: A Stochastic Kinetics Simulator. *Available at hinsberg. net/kinetiscope* **2017**.

(49) Wiegel, A. A.; Wilson, K. R.; Hinsberg, W. D.; Houle, F. A. Stochastic Methods for Aerosol Chemistry: A Compact Molecular Description of Functionalization and Fragmentation in the Heterogeneous Oxidation of Squalane Aerosol by OH Radicals. *Phys. Chem. Chem. Phys.* **2015**, *17* (6), 4398–4411.

(50) Rapf, R. J.; Dooley, M. R.; Kappes, K.; Perkins, R. J.; Vaida, V. pH Dependence of the Aqueous Photochemistry of α-Keto Acids. *J. Phys. Chem. A* **2017**, *121* (44), 8368–8379.

(51) Vargaftik, N. B.; Volkov, B. N.; Voljak, L. D. International Tables of the Surface Tension of Water. *Journal of Physical and Chemical Reference Data* **1983**, *12* (3), 817–820.

(52) Bleys, G.; Joos, P. Adsorption Kinetics of Bolaform Surfactants at the Air/Water Interface.

J. Phys. Chem. **1985**, *89* (6), 1027–1032.

(53) Hołyst, R.; Litniewski, M.; Jakubczyk, D. A Molecular Dynamics Test of the Hertz–Knudsen Equation for Evaporating Liquids. *Soft Matter* **2015**, *11* (36), 7201–7206.

(54) Persad, A. H.; Ward, C. A. Expressions for the Evaporation and Condensation Coefficients in the Hertz-Knudsen Relation. *Chem. Rev.* **2016**, *116* (14), 7727–7767.

(55) Seinfeld, J. H.; Kleindienst, T. E.; Edney, E. O.; Cohen, J. B. Aerosol Growth in a Steady-State, Continuous Flow Chamber: Application to Studies of Secondary Aerosol Formation. *Aerosol Science and Technology* **2003**, *37* (9), 728–734.

(56) Che, D. L.; Smith, J. D.; Leone, S. R.; Ahmed, M.; Wilson, K. R. Quantifying the Reactive Uptake of OH by Organic Aerosols in a Continuous Flow Stirred Tank Reactor. *Phys. Chem. Chem. Phys.* **2009**, *11* (36), 7885.

(57) Vannoy, K. J.; Edwards, M. Q.; Renault, C.; Dick, J. E. An Electrochemical Perspective on Reaction Acceleration in Droplets. *Annual Review of Analytical Chemistry* **2024**.

(58) Lesnicki, D.; Wank, V.; Cyran, J. D.; Backus, E. H. G.; Sulpizi, M. Lower Degree of Dissociation of Pyruvic Acid at Water Surfaces than in Bulk. *Phys. Chem. Chem. Phys.* **2022**, *24* (22), 13510–13513.

(59) Kusaka, R.; Nihonyanagi, S.; Tahara, T. The Photochemical Reaction of Phenol Becomes Ultrafast at the Air–Water Interface. *Nat. Chem.* **2021**, *13* (4), 306–311.

(60) Ahmed, M.; Lu, W. Probing Complex Chemical Processes at the Molecular Level with Vibrational Spectroscopy and X-Ray Tools. *J. Phys. Chem. Lett.* **2023**, *14* (41), 9265–9278.

(61) Kim, P.; Weeraratna, C.; Nemšák, S.; Dias, N.; Lemmens, A. K.; Wilson, K. R.; Ahmed, M. Interfacial Nanostructure and Hydrogen Bond Networks of Choline Chloride and Glycerol Mixtures Probed with X-Ray and Vibrational Spectroscopies. *J. Phys. Chem. Lett.* **2024**, *15* (11), 3002–3010.

(62) Saak, C.-M.; Backus, E. H. G. The Role of Sum-Frequency Generation Spectroscopy in Understanding On-Surface Reactions and Dynamics in Atmospheric Model-Systems. *J. Phys. Chem. Lett.* **2024**, *15* (17), 4546–4559.